Evaluation of Micro- and Nanoscale Uniformity in All-PVD Cu(In,Ga)Se$_2$ Solar Cells

Gregory M. Kimball, Neil Mackie, Magdalena Parker, Atiye Bayman

MiaSolé Hi-Tech Corp., Santa Clara, California 95051, United States.

Abstract – **Over the past several years, advances in manufacturing for thin film Cu(In,Ga)Se$_2$ (CIGS) devices have enabled volume production of high efficiency solar material with good repeatability and uniformity. In this study, quantitative analysis of several advanced imaging techniques was used to evaluate the uniformity of electronic properties for all-PVD CIGS solar cells. Combined EL and DLIT analysis suggests that series resistance in the top electrode constitutes the strongest nonuniformity, which is estimated to contribute about 2.5% relative efficiency loss. High-resolution EL image analysis shows a highly uniform lateral band gap distribution with standard deviations of minimum band gap values <2 meV. Finally, EBIC image analysis shows collection lengths of 1.5 ± 0.2 μm, indicating high collection probability throughout the depth of the CIGS absorber layer and at grain boundaries. Highly uniform micro- and nanoscale electronic properties have enabled all-PVD CIGS solar modules to reach a certified efficiency of 15.7% over 0.97 m^2 aperture area.**

Index Terms – **CIGS, EL, DLIT, EBIC, uniformity**

I. INTRODUCTION

Over the past several years, advances in manufacturing for thin film Cu(In,Ga)Se$_2$ (CIGS) devices have enabled volume production of high efficiency solar material with good repeatability and uniformity. MiaSolé uses thin film CIGS technology based on a "roll-to-cell" platform where all the films that comprise the CIGS solar cell are deposited sequentially onto a flexible stainless steel substrate in a single tool [1]. One difference of this approach compared to other manufacturing methods is the replacement of the typical CdS chemical bath deposition (CBD) layer with a PVD CdS deposition of the buffer layer. The effective process control and repeatability of PVD manufacturing has enabled the production of high-efficiency CIGS solar modules reaching a certified efficiency of 15.7% over 0.97 m^2 aperture area [2].

Several quantitative approaches have been described to assess the effects of local nonuniformities on solar cell performance. Microscale nonuniformities have been investigated using dark lock-in thermography (DLIT) and electroluminescence (EL) to reveal detailed maps of electronic properties [3]. These studies have largely focused on the behavior of crystalline Si solar cells, although some monolithic thin film solar modules have also been assessed [4].

Nanoscale nonuniformities have been studied using cross-sectional electron-beam induced current (EBIC) to estimate the electronic properties of individual grains in a polycrystalline semiconductor [5].

In this study, combined analysis of DLIT and EL images provides a quantitative analysis of series resistance losses in the top electrode, as well as an upper limit on lateral band gap nonuniformity. Cross-sectional EBIC analysis provides information about the distribution of the collection lengths observed for individual crystalline domains. Both microscale and nanoscale electronic properties are shown to be highly uniform.

II. EXPERIMENTAL

DLIT and EL images were collected using a FLIR A315 microbolometer and a Sensovation CoolSamBa HR830 silicon CCD, respectively. EL images were collected using two cycles of image acquisition and background substraction, and a measurement time of 10 sec. DLIT images were collected using sixty cycles of image acquisition with a 3 sec period and 30 frames per sec. Both DLIT and EL images were collected in constant current mode. The EL images were collected at 22 μm/pixel, whereas the DLIT images were collected at 300 μm/pixel and interpolated to provide pixel-to-pixel alignment.

Cross-sectional EBIC samples were prepared by mechanical cleavage and analyzed using a JEOL scanning electron microscope (SEM). The EBIC measurements were conducted with 5–30 keV accelerating voltage, a beam current of 46 pA, and signal amplification using a Stanford Research Systems Low-Current Amplifier.
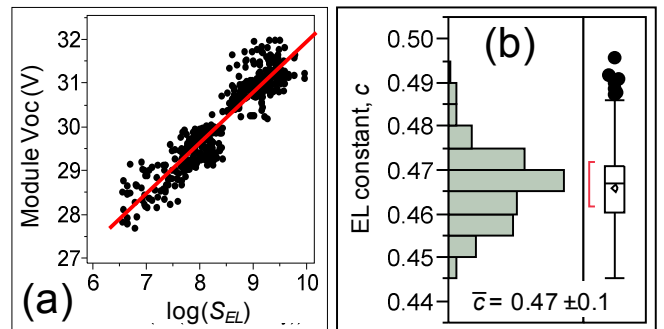

Fig. 1: (a) Average EL signal intensity, or S_{EL}, and Voc data from a series of solar modules studied at 1-sun injection level. (b) the distribution of values for the proportionality constant, c, from (1) derived using the data in Fig. 1a.
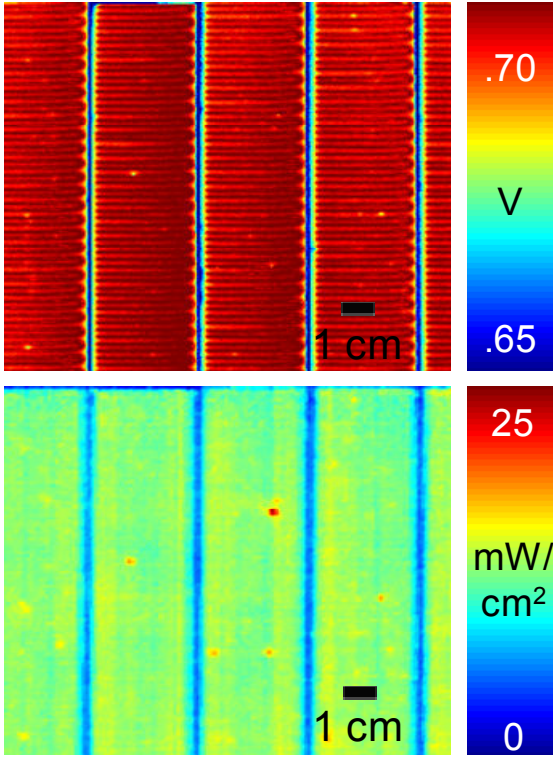
Fig. 2: Images of a CIGS solar module including (a) EL image scaled to show the local voltage, $V_{loc}(x,y)$, based on Fig. 1 and (b) DLIT image scaled to show local power dissipation, $P_{loc}(x,y)$.

Fig. 3: Derived images of a CIGS module including (a) local series resistance map, $R_{S,loc}(x,y)$, and (b) local efficiency map based on electrically-isolated pixels assuming $R_{S,loc}(x,y)$ values.

III. DATA AND RESULTS

Fig. 1a shows the EL intensity and Voc data from population of >500 modules, where EL images were collected at 23 mA/cm^2 forward bias injection and Voc was measured at 1-sun illumination. The data shows a good correlation between the natural logarithm of EL intensity and module Voc across a range of process conditions, and can be modeled using the following relation [6]:

$$V_{oc} = \frac{kT}{q} \ln[S_{EL}] + c \qquad (1)$$

where S_{EL} is the signal intensity from EL, kT/q is the thermal voltage, and c is a proportionality constant. Fig. 1b shows the mean value of c derived for the population of modules. Module V_{oc} has been divided by the number of series-connected cells to provide an averaged relationship between S_{EL} and V_{oc}.

Fig. 2 and 3 show the results of EL and DLIT image analysis for an 8-cell submodule with 1092 cm^2 aperture area built using typical production cells and imaged under 18 mA/cm^2 forward bias. Fig. 2a shows a scaled EL image that reflects the local voltage, $V_{loc}(x,y)$, across the absorber layer. The scaling procedure assumes that variations in EL intensity are predominantly due to the effects of series and shunt resistance, rather than variability in band gap and collection length [3] [7]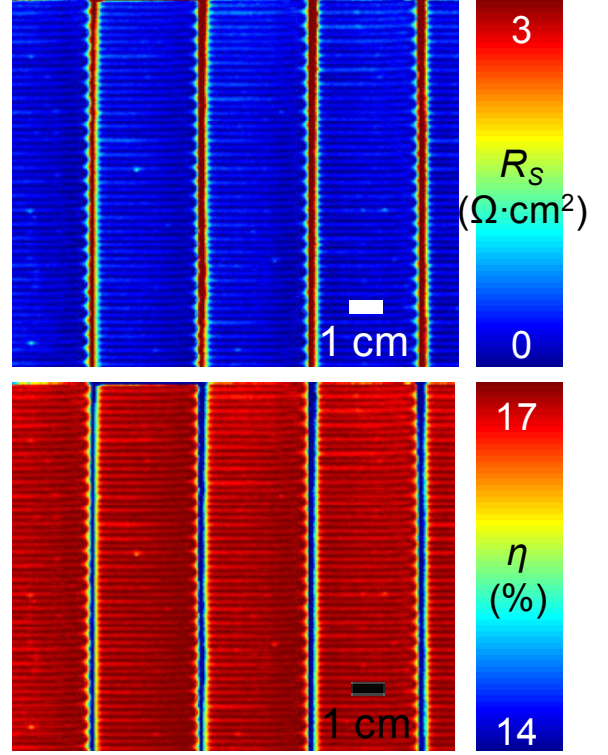. Fig. 2b shows a typical DLIT image that has been scaled to reflect the local power dissipation, $P_{loc}(x,y)$, across the solar cell. The scaling procedure determines the total power dissipated by the module from the dark IV curve and then computes local estimates of power dissipation.

Fig. 3a shows the series resistance map, $R_{s,loc}$, derived from the local voltage and local power dissipation maps in Fig. 2 where values are computed pixel-by-pixel using the following relation:

$$R_{S,loc}(x,y) = [V_{app} - V_{loc}(x,y)]\frac{V_{loc}(x,y)}{P_{loc}(x,y)} \qquad (2)$$

where V_{app} is the external applied voltage. The efficiency map presented in Fig. 3b is constructed by taking each pixel as an electrically-isolated solar cell with the series resistance derived in Fig. 3a. The hypothetical efficiency of each pixel is then calculated using a one-diode PV model incorporating parasitic series resistance.

Fig. 4a shows high-resolution EL imaging of an 8-cell submodule for which intensity linescans were compiled to provide estimates of the intensity standard deviation across a 10 cm^2 area of the submodule. The EL intensity variability was used to estimate variability in lateral minimum band gap values by the following relation [8]:

$$\frac{\sigma S_{EL}}{S_{EL}} = \sqrt{\left(e^{\left[\frac{\sigma_{E_g}^2}{k^2 T^2}\right]} - 1\right)} \qquad (3)$$

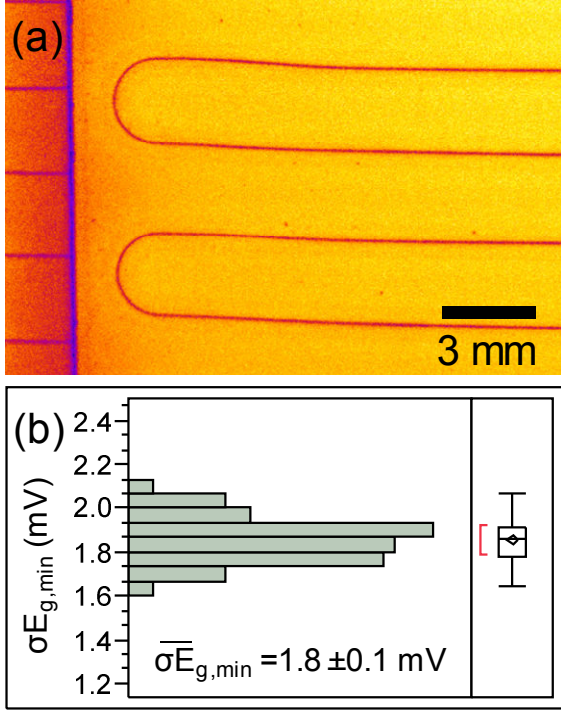Fig. 4: EL analysis of a CIGS solar module including (a) EL image collected at 6 mA/cm² for high-resolution intensity analysis and (b) distribution of $\sigma E_{g,min}$ values assuming that the EL signal variation within the image is driven by band gap variation.
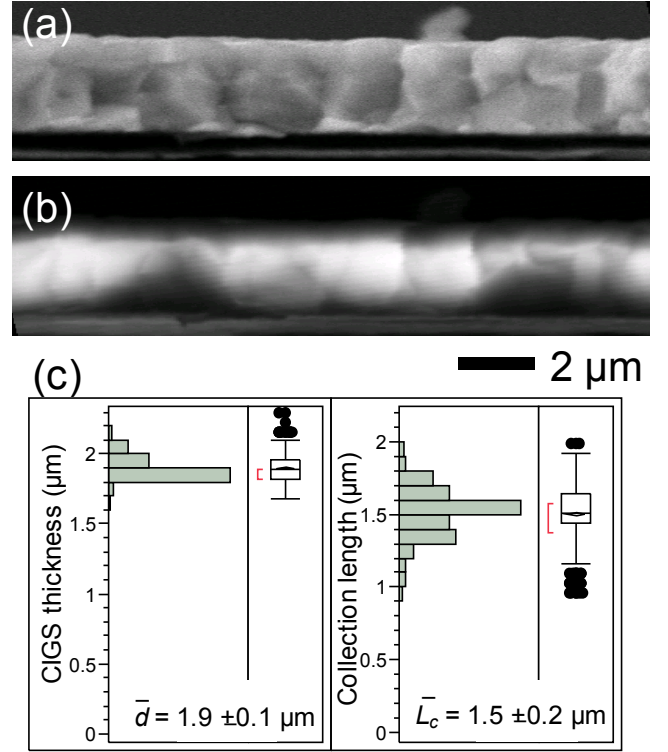

Fig. 4: Cross-section of CIGS device layer including (a) SEM and (b) EBIC images. (c) Analysis of the SEM and EBIC profiles provides distributions of CIGS absorber layer thickness, d, (left) and collection length, L_c, (right) estimated across a cross-section width of 100 μm.

where σS_{EL} is the standard deviation of EL signal intensity and σE_g is the standard deviation of minimum band gap values.

Fig. 5a and 5b show cross-sectional SEM and EBIC images over the same region of a CIGS device layer. Fig. 5c shows the distribution of film thicknesses as determined by image analysis, and the distribution of collection lengths as determined using the analytical treatment described in the literature [5]:

$$I(a) = \int_0^\infty g(x,a)f_c(x)\mathrm{d}x \qquad (4)$$

where $I(a)$ represents the measured EBIC signal at beam position, a, and $g(x,a)$ represents the generation profile of excess minority carriers at the depth of the film, x, generated by the electron beam at position, a, and $f_c(x)$ represents the collection probability function of the device under test. The assumptions of film thickness, depletion width, W_D, and electron diffusion length, L_e, were allowed to vary in the model and collection lengths are reported as the sum, $W_D + L_e$.

IV. DISCUSSION

The series resistance and efficiency maps shown in Fig. 3 can be used to estimate the efficiency loss due to series resistance in the top electrode. Fig. 3a implies a mean series resistance value of 0.33 Ω·cm², whereas previous reports of monocrystalline Si solar cells estimated a mean series resistance value of 0.42 Ω·cm² by the same technique [3]. The efficiency map implies a maximum efficiency of 17.2% and an average efficiency of 16.8%, which corresponds to a 0.4% absolute (2.5% relative) efficiency loss due to series resistance losses in the top electrode. Mean efficiency data from the derived image Fig. 3b suggests that series resistance associated with wire-to-wire spacing and with cell edge-to-wire spacing contribute about equally to overall series resistance losses [4].

The EL image in Fig. 4a was used to estimate the lateral variation in minimum band gap values across the cell with about 22 μm/pixel resolution. Fig. 4b shows the results of >100 EL linescans across the submodule for which the standard deviation in S_{EL} within a linescan was found to be about 7% of the mean value, implying a standard deviation in E_g of 1.8 ± 0.1 meV by the relation (3). This result compares favorably to a similar estimate of <4 meV from the literature [7]. Furthermore, the all-PVD CIGS device stack does not show evidence of secondary diode effects characteristic of devices incorporating CBD CdS in the high-resolution EL images [7], confirming uniform electronic properties across the device.

Although the literature describes cross-sectional EBIC analysis based on CIGS properties or deposition conditions, the systematic analysis of collection length across a series of

grains has not typically been reported. The collection length distribution presented here shows values >1 μm for essentially all grains, and does not show significant collection loss at grain boundaries.

V. SUMMARY

Quantitative analysis of several advanced imaging techniques was used to evaluate the uniformity of electronic properties for all-PVD CIGS solar cells. Series resistance in the top electrode constitutes the strongest nonuniformity, and is estimated to contribute about 2.5% relative efficiency loss. EL analysis shows highly uniform lateral band gap distribution with a standard deviation of minimum band gap values <2 meV. EBIC analysis shows collection lengths of 1.5 ± 0.2 μm, indicating high collection probability throughout the depth of the CIGS absorber layer and at grain boundaries.

REFERENCES

[1] N. Mackie, R. Tas, J. Corson, and A. Bayman, "A Different Approach: CIGS using All PVD," in *28th European PV Solar Energy Conference*, Paris, 2013, p. 3AO.4.1.

[2] M. A. Green, K. Emery, Y. Hishikawa, W. Warta, and D. Dunlop, "Solar cell efficiency tables (version 43)," *Progress in Photovoltaics*, vol. 22, pp. 1-9, 2014.

[3] K. Ramspeck et al., "Recombination current and series resistance imaging of solar cells by combined luminescence and lock-in thermography," *Applied Physics Letters*, vol. 90, p. 153502, 2007.

[4] A. Helbig, T. Kirchartz, R. Schaeffler, J. Werner, and U. Rau, "Quantitative electroluminescence analysis of resistive losses in Cu(In,Ga)Se2 thin-film modules," *Solar Energy Materials & Solar Cells*, vol. 94, pp. 979-984, 2010.

[5] M. Nichterwitz, *Charge carrier transport in Cu(In,Ga)Se2 thin-film solar-cells studied by electron beam induced current*. Berlin: PhD Thesis, 2012.

[6] U. Rau, "Reciprocy relation between photovoltaic quantum efficiency and electroluminescent emission of solar cells," *Physical Review B*, vol. 76, p. 085303, 2007.

[7] G. Brown, V. Faifer, B. Cardozo, E. Bykov, and M. Contreras, "Theory of electroluminescence intensity and insights into recombination in thin films solar cells," *Applied Physics Letters*, vol. 96, p. 222102, 2010.

[8] A. Pudov, B. Cardozo, V. Faifer, E. Bykov, M. Contreras G. Brown, "Quantitative imaging of electronic nonuniformities in Cu(In,Ga)Se2 solar cells," *Journal of Applied Physics*, vol. 108, p. 074516, 2010.